

## RESEARCH ARTICLE

## MEDICAL PHYSICS

# Evaluation of inverse treatment planning for gamma knife radiosurgery using fMRI brain activation maps as organs at risk

David Abramian<sup>1,2</sup> | Ida Blystad<sup>2,3</sup> | Anders Eklund<sup>1,2,4</sup>

<sup>1</sup>Division of Medical Informatics, Department of Biomedical Engineering, Linköping University, Linköping, Sweden

<sup>2</sup>Center for Medical Image Science and Visualization (CMIV), Linköping University, Linköping, Sweden

<sup>3</sup>Department of Radiology in Linköping and Department of Health, Medicine and Caring Sciences, Linköping University, Linköping, Sweden

<sup>4</sup>Division of Statistics & Machine Learning, Department of Computer and Information Science, Linköping University, Linköping, Sweden

## Correspondence

Anders Eklund, Division of Medical Informatics, Department of Biomedical Engineering, Linköping University, Linköping, Sweden.

Email: [anders.eklund@liu.se](mailto:anders.eklund@liu.se)

## Funding information

Centrum för Industriell Informationsteknologi, Linköpings Universitet; Vinnova, Grant/Award Numbers: 2018-02230, 2021-01954; LiU Cancer

## Abstract

**Background:** Stereotactic radiosurgery (SRS) can be an effective primary or adjuvant treatment option for intracranial tumors. However, it carries risks of various radiation toxicities, which can lead to functional deficits for the patients. Current inverse planning algorithms for SRS provide an efficient way for sparing organs at risk (OARs) by setting maximum radiation dose constraints in the treatment planning process.

**Purpose:** We propose using activation maps from functional MRI (fMRI) to map the eloquent regions of the brain and define functional OARs (fOARs) for Gamma Knife SRS treatment planning.

**Methods:** We implemented a pipeline for analyzing patient fMRI data, generating fOARs from the resulting activation maps, and loading them onto the GammaPlan treatment planning software. We used the Lightning inverse planner to generate multiple treatment plans from open MRI data of five subjects, and evaluated the effects of incorporating the proposed fOARs.

**Results:** The Lightning optimizer designs treatment plans with high conformity to the specified parameters. Setting maximum dose constraints on fOARs successfully limits the radiation dose incident on them, but can have a negative impact on treatment plan quality metrics. By masking out fOAR voxels surrounding the tumor target it is possible to achieve high quality treatment plans while controlling the radiation dose on fOARs.

**Conclusions:** The proposed method can effectively reduce the radiation dose incident on the eloquent brain areas during Gamma Knife SRS of brain tumors.

## KEYWORDS

functional MRI, gamma knife, treatment planning

## 1 | INTRODUCTION

Brain tumors compose about 2% of new cancer diagnoses, affecting some 300 000 subjects globally each year.<sup>1</sup> Although not the most prevalent cancer type, brain tumors are prone to complicated and challenging treatment procedures, which often combine surgical resection, radiotherapy, and chemotherapy, with a high morbidity and low survival rate for the patients. Stereotactic radiosurgery (SRS) can be an efficient treatment

option for small primary brain tumors and metastases. However, treatment planning requires considerable time, as it involves collecting MR and/or CT images, segmenting the tumor and organs at risk (OARs), and the generation of treatment plans. Furthermore, OARs typically include various anatomical landmarks, but eloquent regions of the brain are rarely used for this purpose. In this work, we describe a workflow for efficiently incorporating functional OARs (fOARs), in the form of brain activation maps derived from functional

This is an open access article under the terms of the [Creative Commons Attribution](https://creativecommons.org/licenses/by/4.0/) License, which permits use, distribution and reproduction in any medium, provided the original work is properly cited.

© 2023 The Authors. *Medical Physics* published by Wiley Periodicals LLC on behalf of American Association of Physicists in Medicine.

MRI (fMRI), into Gamma Knife SRS treatment planning in order to minimize the radiation dose incident on eloquent brain areas.

## 1.1 | Stereotactic radiosurgery

SRS is an image-guided non-invasive surgical approach which relies on focused beams of radiation to ablate tissue. Originally developed to treat various benign intracranial conditions, it has since seen its use extended to malignant conditions, both intracranial and elsewhere in the body.

Since its inception, SRS has been adopted within the fields of neurosurgery and radiation oncology. It has become one of the treatments of choice for multiple intracranial conditions and malignancies, such as arteriovenous malformations, vestibular schwannomas, cavernous sinus meningiomas, recurrent or residual pituitary tumors, metastatic tumors, and trigeminal neuralgia.<sup>2</sup> It is also increasingly being applied for the treatment of high- and low-grade gliomas<sup>3–6</sup> and meningiomas.<sup>7–9</sup>

## 1.2 | Handling risk organs

Despite the precise dose delivery and sharp dose fall-off achievable with radiosurgery, patients are still at risk of suffering various radiation-induced toxicities. Complications associated with SRS for vestibular schwannoma include facial neuropathy, hearing loss and damage to the trigeminal nerve.<sup>10</sup> High grade glioma treatment complications include radionecrosis, cranial nerve palsy, paralysis, seizures, CNS hemorrhage, and stroke.<sup>3</sup> A large scale meta-analysis of published research on Gamma Knife radiosurgery for arteriovenous malformations found that 34% of the patients developed radiation-induced changes, with 8% developing neurological symptoms and 3% experiencing permanent neurologic deterioration.<sup>11</sup> A study on SRS for brain metastases found that new neurological and non-neurological complications were associated with 40% of SRS treatments for brain metastases, and that patients with lesions in functional brain regions have a significantly increased risk of treatment-related complications.<sup>12</sup> These complications include motor deficit, headache, visual deficit, sensory deficit, cognitive deficit, seizure, ataxia, memory deficit, dizziness, cranial nerve dysfunction, gait disturbance, and speech dysfunction.

In order to mitigate potential radiation-induced functional deficits to patients treated with SRS, it is common to segment various OARs during the treatment planning process, and keep the dose incident on them within established limits by shaping the radiation dose

delivered to the targets. For SRS of the brain, these OARs typically include anatomical regions such as the brain stem, the hippocampus, the optic nerves, and the cochlea.

## 1.3 | Using risk organs from functional MRI

Since its development in 1992, fMRI has been used to study brain activity and brain connectivity.<sup>13</sup> It has become very popular for both research and clinical applications, as it is based on a natural contrast mechanism that is part of the human physiology.

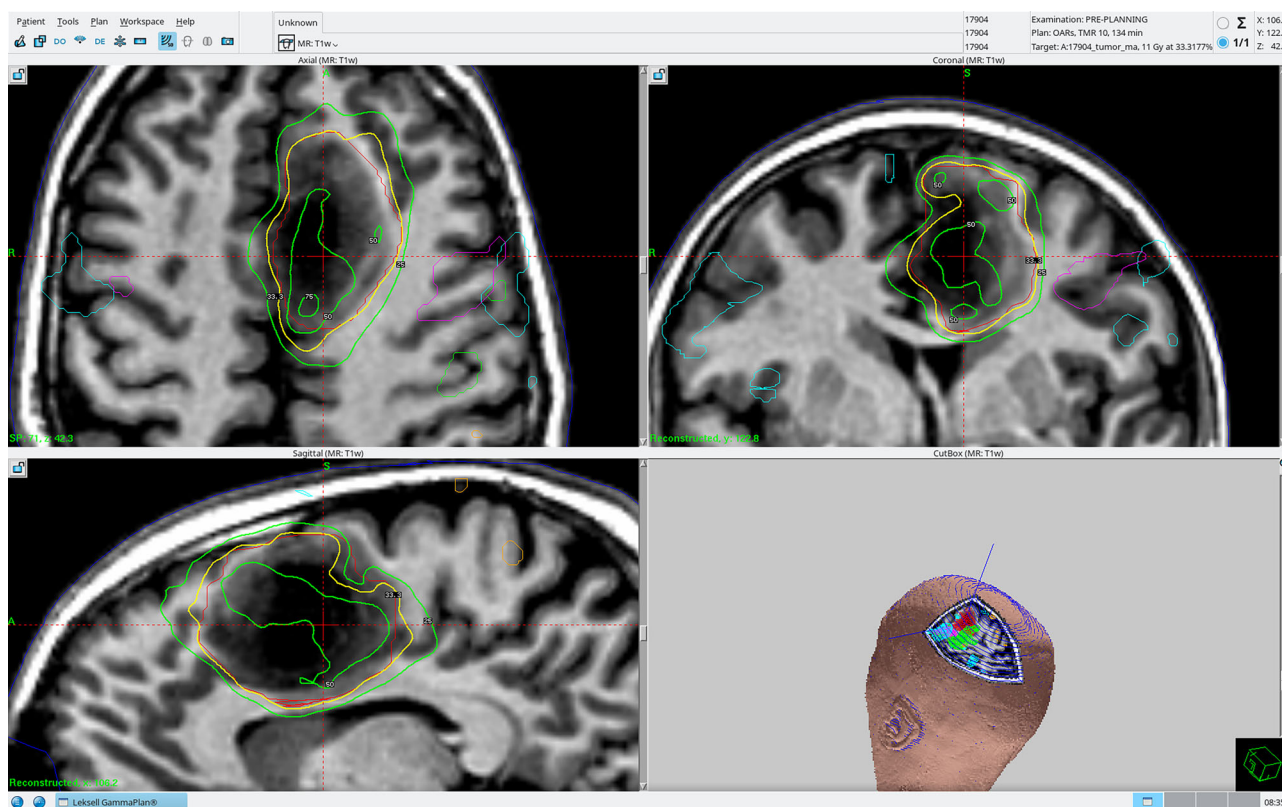
Table 1 summarizes previous radiotherapy and radiosurgery work using supplementary imaging modalities, such as fMRI and diffusion tensor imaging (DTI), to specify additional OARs not identifiable in conventional anatomical imaging protocols. fOARs derived from fMRI have been previously used to spare the eloquent brain regions in radiotherapy,<sup>14–16</sup> as well as in SRS with LINAC<sup>17–19</sup> and CyberKnife,<sup>20–23</sup> but, to the best of our knowledge, not with Gamma Knife, where the focus has been on sparing critical white matter fiber bundles by incorporating DTI tractography into treatment planning<sup>24–28</sup> (see Table 1). One reason for this could be the availability of inverse planning solutions. While treatment plans with multiple anatomical and/or functional OARs can be designed with manual forward planning, the process can be too time-consuming, depending on the number and size of the targets and the OARs, as well as the distances between them. Modern inverse planning methods for radiation delivery<sup>29–31</sup> greatly simplify the incorporation of fOARs into the treatment planning routine, using automatic optimization to generate treatment plans that consider multiple OARs within minutes. The recent introduction of the Elekta Gamma Knife Lightning treatment planner<sup>29</sup> (henceforth referred to as Lightning) enables the creation of complex treatment plans with multiple OARs for Gamma Knife SRS.

The main purpose of this paper is to show that it is possible to automatically process fMRI data from brain tumor patients, and to automatically convert the results into a format which can be read by GammaPlan. We have therefore developed a pipeline for analyzing fMRI data to create fOARs, and converting the anatomical images and fOARs into DICOM objects that can be imported into the Elekta Leksell GammaPlan software (henceforth referred to as GammaPlan, see Figure 1), to be used with the Lightning inverse planner add-on. We used this pipeline to generate retrospective treatment plans for five brain tumor patients and evaluated the effects of including fOARs in the treatment planning process with the Lightning planner.

**TABLE 1** Summary of existing publications using supplementary imaging modalities to define organs at risk for radiation treatment planning.

Reference	Imaging modalities	Number of patients	Delivery	Condition
Narayana et al. 2007	fMRI, MRSI	12	IMRT	Glioma
Kovács et al. 2011	fMRI	20	3DCRT, IMRT	Glioma
Wang et al. 2015	fMRI, DTI tractography	20	3DCRT, IMRT	Glioma
Hamilton et al. 1997	fMRI, SPECT	2	LINAC SRS	Various
Schulder et al. 2000	fMRI	12	LINAC SRS	Various
Liu et al. 2000	fMRI	3	LINAC SRS	Various
Stancanello et al. 2007	fMRI	5	CyberKnife	AVM
Pantelis et al. 2010	fMRI, DTI tractography	4	CyberKnife	Various
Conti et al. 2013	fMRI, DTI tractography, NBS	25	CyberKnife	Various
De Martin et al. 2017	fMRI, MEG	4	CyberKnife	Metastases
Maruyama et al. 2005	DTI tractography	7	Gamma Knife	AVM
Maruyama et al. 2007	DTI tractography	10	Gamma Knife	AVM
Maruyama et al. 2009	DTI tractography	12	Gamma Knife	AVM
Koga et al. 2012	DTI tractography	144	Gamma Knife	AVM
Gavin and Sabin 2016	DTI tractography	20	Gamma Knife	Various

Abbreviations: 3DCRT, 3D conformal radiation therapy; AVM, arteriovenous malformation; DTI, diffusion tensor imaging; fMRI, functional magnetic resonance imaging; IMRT, intensity modulated radiation therapy; LINAC, linear accelerator; MEG, magnetoencephalography; MRSI, magnetic resonance spectroscopic imaging; NBS, navigated brain stimulation; SPECT, single-photon emission computed tomography.

**FIGURE 1** An example of treatment planning in GammaPlan after loading the anatomical images, the tumor mask and the risk organs obtained from fMRI. Red contours represent the tumor mask. Thick yellow and green contours represent the 11 and 4 Gy isodose levels, respectively, corresponding to the target tumor irradiation dose and the maximum dose constraint on fOARs, respectively. Thin green, orange, cyan, and magenta contours represent fOARs defined from the hand, foot, lips and verb repetition fMRI conditions, respectively. fMRI, functional MRI; fOARs, functional organs at risk.

**TABLE 2** An overview of the patients analyzed in this study. Patients with tumors larger than 40 cm<sup>3</sup> were excluded from the original Pernet et al. dataset, since Stereotactic radiosurgery is normally not used for such patients. Not all fMRI datasets are available for all patients.

Subject ID	Pathology	Tumor location	Tumor size (cc)	Available fMRI data
17904	Oligodendroglioma type II	Left supplementary motor area	35.92	M V R
18582	Astrocytoma type II	Wernicke area	10.34	M V W
18975	Glioblastoma multiforme	Left primary motor area	13.24	M V W R
19015	Glioblastoma multiforme	Left supplementary motor area	37.40	M V W
19849	Not available	Right primary motor area	9.66	M R

Abbreviations: M, motor; R, resting state; V, verb generation; W, word repetition.

**TABLE 3** Acquisition parameters for the Pernet et al. dataset.

Parameter	T1w	Motor	Verb generation	Word repetition
Voxel size (mm)	1 x 1.3 x 1	4 x 4 x 4	4 x 4 x 4	4 x 4 x 4
Dimensions (voxels)	256 x 156 x 256	64 x 64 x 30	64 x 64 x 30	64 x 64 x 30
TR (s)	10	2.5	2.5	5 (effective 2.5)
Number of volumes	1	184	173	76

## 2 | DATA

We used an open MRI dataset of brain tumor patients to carry out our experiments.<sup>32</sup> The dataset contains structural (T1w, T2w, DWI) and functional MRI data from 22 patients with various types of brain tumors located close to the eloquent regions of the brain. Functional imaging protocols include a motor task consisting of three conditions (finger tapping, foot flexing, lip pursing), a covert verb generation task (mapping of Broca area and supplementary motor area), an overt word repetition task (mapping of Wernicke area), as well as resting state fMRI. The employed fMRI protocol has previously been shown to provide reliable single-subject activations on control subjects.<sup>33</sup> Due to medical considerations, not all fMRI datasets are available for all patients. While we are aware of larger open brain tumor datasets, such as the BraTS dataset,<sup>34</sup> including 1251 subjects in the training set of the 2021 version, they do not generally include fMRI data, and are thus unsuitable for this work.

Due to limitations in the suitable radiation doses and treatment times for a patient, SRS is mainly applied on relatively small pathologies. Because of this, we only used data from patients with tumors smaller than 40 cm<sup>3</sup>, which excluded 17 of the 22 patients in the dataset. Table 2 presents information on the remaining five subjects that were used in our analyses.

For each subject we made use of the T1w volume as reference for treatment planning, and the task fMRI data was used to obtain functional OARs (fOARs). Table 3 presents some relevant acquisition parameters for these modalities. While the dataset includes tumor masks, these were generated using a semi-automatic proce-

dures. To ensure the accurate localization of the tumors, co-author IB, an experienced neuroradiologist, manually annotated the tumor for each of the patients used in our analyses.

## 3 | METHODS

This section describes the methods used to generate the fMRI activation maps and use them as fOARs for treatment planning in GammaPlan. All data processing and conversion was done using a combination of Bash, Matlab, and Python scripts, which are available online.<sup>1</sup> A diagram of our processing and analysis pipeline is shown in Figure 2.

### 3.1 | Preprocessing of MRI data

For each subject, the T1w and fMRI data are available in NiftI format. The first four volumes of all fMRI sequences are dummy volumes, and were deleted. We chose to preprocess the anatomical and functional MRI data with the fMRIPrep software,<sup>35</sup> which purposefully combines processing steps from multiple MRI software tools to produce a robust and versatile preprocessing pipeline in accordance with best practices. As fMRIPrep requires the data to be in the BIDS format,<sup>36</sup> the dataset was first manually converted to BIDS. The preprocessing steps included bias correction of the T1w volume, brain mask extraction, head motion correction of the fMRI volumes, and co-registration of fMRI data to the

<sup>1</sup> <https://github.com/DavidAbramian/CENIT2>



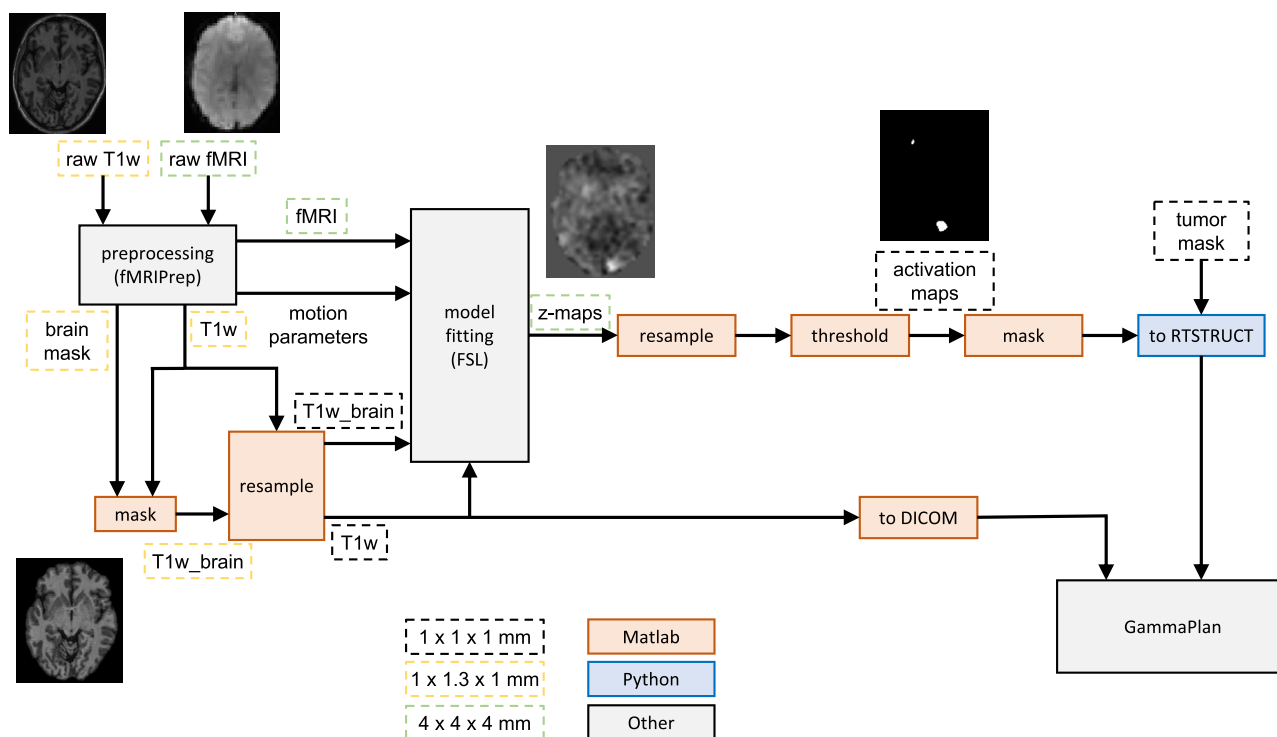


**FIGURE 2** Diagram of the preprocessing and statistical analysis pipeline for fMRI data. The preprocessing (e.g., registration between T1w and fMRI volumes, head motion correction) is done with the fMRIPrep software, with some additional resampling of the volumes. The statistical analysis of the fMRI data is done with the FSL software. A custom Python script is finally used to convert the brain activity maps to DICOM RTSTRUCT, for loading them into GammaPlan. fMRI, functional MRI.

corresponding T1w anatomical references, among others. A full description of the preprocessing performed by fMRIPrep is given in the Appendix.

We experimented with several different settings for fMRIPrep with and without the inclusion of brain surface extraction with FreeSurfer<sup>37</sup> for the refinement of the brain mask. Given the substantial increase in processing time from the use of surface extraction (6 hours per subject vs. 1.5 hour per subject) and the minimal differences observed in the final results, we decided not to use surface processing for our experiments. Other fMRIPrep settings used included producing output in the native space of each subject, and using experimental fieldmap-free susceptibility distortion correction for the fMRI data, due to the absence of fieldmaps in the dataset.

Following preprocessing with fMRIPrep, we used the generated brain mask to produce a skull-stripped version of the T1w volume, to be used in FSL. Both versions of the T1w volume were then resampled to 1 mm isotropic resolution and  $256 \times 256 \times 256$  voxels in order to fulfill a requirement from the GammaPlan software, namely that the 2D slices of the reference volume have square pixels. These images were used by co-author IB to produce new tumor segmentations, so these were made in the target resolution.

### 3.2 | Activation mapping

We used the FSL 6.0.4 software<sup>38</sup> to perform first-level analysis of the fMRI data. Preprocessing steps were disabled, as they were already carried out by fMRIPrep, with the exception of spatial smoothing. Due to the importance that smoothing has for the detection power and spatial specificity of found activations, we decided to test Gaussian filters of two different sizes for our analyses, with full width at half maximum (FWHM) sizes of 4 and 6 mm, respectively. The GLM design matrices included an activity regressor for each task, the temporal derivative of each activity regressor, and a standard set of six head motion regressors estimated by fMRIPrep.

Prior to thresholding the Z-static maps, these were resampled to the same resolution of the T1w reference volume, as necessary setup for the later conversion of the activation maps into DICOM RTSTRUCT formatted data (see Section 3.4). The resampled Z-statistic maps were then thresholded at an arbitrary voxel level of  $Z = 5$ , with no cluster extent threshold, to produce binary activation maps. While arbitrary, this threshold provides relatively strong family-wise error control, corresponding to Bonferroni correction with  $\alpha$  between 0.006 and 0.008 for the various subjects and tasks. This activation mapping scheme did not produce any activations

for the word repetition task for any subject, so this task was disregarded in the remainder of our analyses.

The arbitrary nature of our chosen thresholding scheme was considered appropriate for several reasons. Firstly, there is currently no consensus on how to best threshold brain activation maps for single subject fMRI analysis. This is especially true for clinical applications, where the relative importance of false positives and false negatives is different to that in research.<sup>39</sup> Furthermore, ad hoc thresholds are routinely used in clinical fMRI, where the operator manually adjusts the thresholds until a satisfactory activation map had been achieved,<sup>40</sup> or sets them in accordance with the relative ease of detecting activations for different tasks.<sup>20</sup> As our work is not focused on settling these questions but on demonstrating the feasibility of generating and using fOARs for Gamma Knife treatment planning, we chose an arbitrary thresholding level with strong control of family-wise error rates.

### 3.3 | Masking of activation maps

For several subjects and tasks, fMRI activations were present inside or in close proximity to the tumor mask. It is unclear whether these activations represent true brain activity or they are artifactual, potentially caused by tumor-induced neurovascular uncoupling.<sup>39,41</sup> However, as the GammaPlan inverse planner treats the maximum dose on OARs as a hard optimization constraint, it prioritizes reducing the radiation dose incident on OARs over fulfilling the irradiation requirements on the tumor mask, resulting in poor quality treatment plans. In order to address this issue, we created three additional masked versions of each activation map: one where activations found inside the tumor mask were removed, and two where activations were also removed within 2 and 4 mm of any tumor voxel, respectively. Thus, for each subject and condition we generated eight activation maps in total (2 smoothing settings  $\times$  4 masking settings).

### 3.4 | Data conversion to DICOM

As a clinical software, the GammaPlan treatment planning software accepts input data in the DICOM format, ensuring interoperability with other medical devices. However, most fMRI processing and analysis tools require data in the NIfTI format, standard in neuroimaging research, so this is the data format used throughout our pipeline. Therefore, a data conversion step was needed before the brain activation maps could be loaded onto GammaPlan.

The various ROIs, such as the tumor mask and activation maps, need to be provided as DICOM radiotherapy structure sets (RTSTRUCTs),<sup>42</sup> used for the storage and transfer of patient structures. In this format ROIs are rep-

resented as collections of contours encompassing the relevant region, with each contour being associated to a reference DICOM object, which in our case are individual T1w axial slices. A single RTSTRUCT file can contain any number of separate ROIs, each of which can be used as a target or risk organ in GammaPlan. Contrastingly, the most common way of representing ROIs in the NIfTI format is as binary volumes, with voxels taking a value of 1 if belonging to the ROI and 0 otherwise.

The T1w reference volume of each subject was split into 256 axial slices, and each of them converted into a DICOM file. The conversion of ROIs from solid 3D regions into collections of 2D contours was done using a custom Python script. The active voxels were first extracted for each axial slice separately, following which the contours enclosing each connected regions were found automatically using the `find_contour` routine from the `scikit-image` package,<sup>43</sup> which relies on the marching squares algorithm for finding contours. The sets of contours were converted into RTSTRUCT files using the `pydicom` package.<sup>44</sup> Specifically, as RTSTRUCT files can be quite complex, we used the `codify` function to deconstruct an existing RTSTRUCT file and generate the Python code that would recreate it, and altered this code to suit our needs.

### 3.5 | Treatment planning

A non-clinical version of GammaPlan<sup>2</sup> was set up on an HP Z6 G4 workstation with a 10 core Intel Xeon 2.2 GHz CPU, an Nvidia Quadro P2000 GPU, and 96 GB of RAM, in accordance with the required specification for the software, with the exception of the increased RAM (96 GB instead of 32 GB). All analyses were performed with a treatment dose rate of 3.5 Gy/min, corresponding to a new Gamma Knife unit.

For each subject, the set of DICOM files containing the T1w reference volume and the RTSTRUCT files containing the tumor mask and activation map ROIs were transferred to the GammaPlan workstation using a USB drive and imported into the software. Each subject and set of parameters were analyzed in separate examinations within the software. For each such examination, the T1w reference volume and relevant tumor and fOAR ROIs were loaded. In all cases, all of the available activation maps for each subject were used simultaneously, yielding between 80 and 180 risk organs (i.e., individual brain activity clusters, see section 5.3). The skull was segmented automatically in GammaPlan from the T1w volume.

We defined two treatment plans in each examination: one where only the target dose for the tumor is specified, and another where dose limits were also set for each

<sup>2</sup> software build: alpha1A1-nonclinical (6576.d71bbebac) @ sesrdtpsbuild005 2019-10-10T11:55

fOAR. The doses incident on the tumor and fOARs were logged in both cases. We used a target dose of 11 Gy and a dose limit of 35 % of the target dose (4 Gy) for all fOARs in all cases.

Optimized treatment plans were generated using the Lightning inverse planning system.<sup>29</sup> It provides two tuning parameters for setting the relative importance of minimizing the dose incident on tissue outside the target and minimizing the beam-on-time, respectively. These were set to their default value of 0.5. The optimization of individual treatment plans took between 20 s and 30 min.

### 3.6 | Exporting GammaPlan results

As treatment plan optimization times are not reported in GammaPlan, we measured them by tracking the timing of changes in on-screen dialog boxes, using motion tracking software running on another computer with a webcam. Furthermore, while it is possible to export complete treatment plans in DICOM format, detailed dose reports for ROIs are only presented in a table to be visualized by the GammaPlan operator, and can not be exported in a machine-readable format on a single-treatment-plan basis. GammaPlan offers the possibility of exporting the full debug logs of the treatment planning computer to external media, which include a complete history of treatment planning logs with detailed statistics in JSON format, but these do not include minimum and mean dose statistics for ROIs other than the targets. In addition, this process is inconvenient for exporting the metrics of individual treatment plans of interest, as it is time-consuming and produces a large number of log files unrelated to this task. Therefore, in order to extract the full treatment planning statistics reported by GammaPlan, we took screenshots of the results tables and exported them as PDF files to a USB drive. We then used custom OCR software written in Matlab to parse the numbers from the tables. The dose statistics for all ROIs that constitute a single fMRI condition were combined.

## 4 | RESULTS

For every subject, spatial filter size, and masking setting, we compared the quality of treatment plans with and without the inclusion of fOARs with different masking settings in the optimization process. In total we generated 50 treatment plans (5 subjects  $\times$  2 smoothing levels  $\times$  (no fOARs + fOARs with 4 masking settings)). Figure 3 shows example treatment plans for every subject and setting tested.

We evaluated the treatment plans on the basis of the metrics reported by GammaPlan. These include minimum, maximum and mean doses for each ROI

(tumor mask and fOARs), as well as the following overall treatment plan quality metrics: target coverage, Pad-dick conformity index (PCI),<sup>45</sup> gradient index,<sup>46</sup> and treatment time. In addition, we report the optimization time needed to produce each treatment plan. Note that GammaPlan did not report gradient indices for the subjects with larger tumors, so results are only provided for subjects 18 582, 18 975 and 19 849.

### 4.1 | Effects of including fOARs

Treatment planning without the inclusion of fOARs results in highly conformal treatment plans, with a target coverage of 1 in all cases, a median PCI of 0.89 (range 0.86 – 0.90), and a median gradient index of 2.66 (range 2.62 – 2.75) where reported. The median minimum, maximum and mean doses delivered to the tumors are 9.9, 20.7 and 15.2 Gy, respectively, reflecting good compliance with the target doses. However, the doses received by the fOARs are in excess of the permissible maximum, with a median maximum dose on fOARs of 6.7 Gy, and reaching doses larger than 10 Gy in several cases.

Incorporating maximum dose constraints for fOARs successfully limits the dose received by them, lowering the median maximum dose on fOARs to 3.9 Gy, that is, just under the maximum constraint of 4 Gy. In spite of that, the presence of fMRI activations within or in close proximity to the tumor masks results in the inclusion of dose constraints for fOARs having a severe detrimental effect on treatment plan metrics. In this case the median target coverage and PCI are reduced to 0.80 (range 0.60 – 0.97) and 0.70 (range 0.48 – 0.81), respectively, while the median gradient index increased to 2.88 (range 2.74 – 3.19). Furthermore, while the mean tumor doses remained approximately constant, the treatment plans suffer from both hot and cold spots, as indicated by high maximum and low minimum doses, with medians of 2.25 and 32.45 Gy, respectively.

As illustrated by visually comparing the treatment plans in the first two columns of Figure 3 (e.g., subjects 17 904, 18 582, and 19 015), the 4 Gy isoline very closely follows the shape of any fMRI activations adjacent to the tumor mask whenever such a dose constraint is set on the fOARs, suggesting that the optimizer is successful in shaping the delivered dose in order to follow the dose constraints imposed on risk organs.

### 4.2 | Effects of masking fMRI activation maps

We tested three masking settings with the goal of separating the closest fMRI activations from the tumor mask and thus improving the quality of the resulting treatment plans.



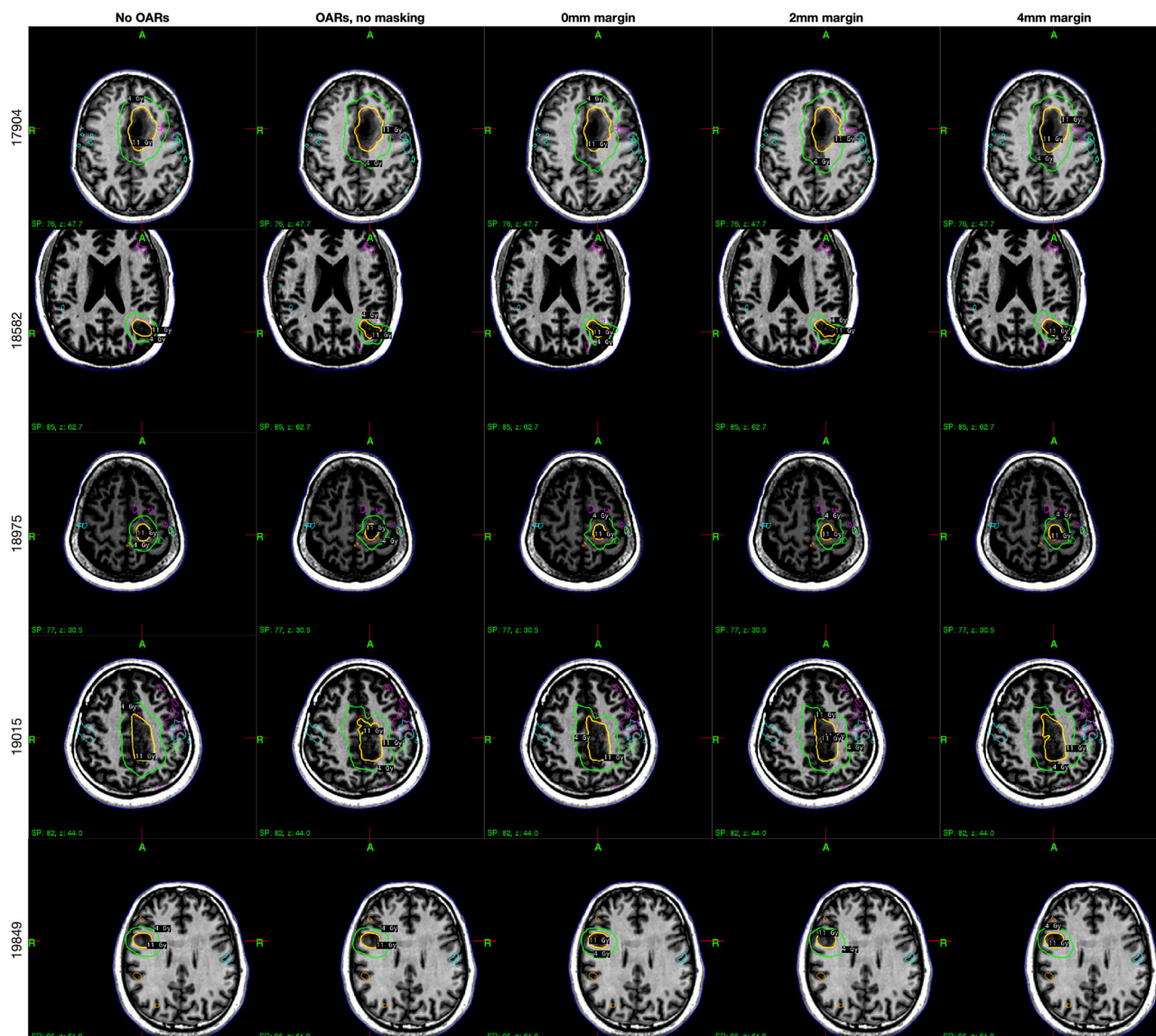


**FIGURE 3** Example treatment plans obtained for all subjects and masking settings, using spatial smoothing with a 4 mm FWHM filter. The first column (“No fOARs”) shows results where no dose limits are set for the fOARs, while the remaining four columns represent the various masking settings employed. Thick yellow and green contours represent the 11 and 4 Gy isolevels, respectively, corresponding to the target tumor irradiation dose and the maximum dose constraint on OARs, respectively. Thin magenta, cyan, orange and green contours represent fOARs defined from each fMRI condition (three from the motor task and one from the verb generation task). fMRI, functional MRI; fOARs, functional organs at risk; FWHM, full width at half maximum; OARs, organs at risk.

Removing all activations that fall inside the tumor results in a slight improvement in the treatment plan metrics, with a median target coverage of 0.83 and a median PCI of 0.73, respectively, while the median gradient index remains at 2.88. The median maximum dose decreases to 30.1 Gy, and the median minimum tumor dose increases to 2.65 Gy, indicating that the hot and cold spots in the treatment plan are somewhat alleviated. Although this constitutes a marked improvement for the treatment plans, most fMRI activations within the tumor mask do not appear deep inside the tumor, but are portions of larger activations adjacent to the tumor which extend into its edges (see Figure 3, sec-

ond and third columns). The remaining portion of such activations, as well as any other activations immediately adjacent to the tumor, would shrink the portion of the tumor receiving the full treatment dose, and have a detrimental effect on the treatment plans.

Masking out all activations within 2 mm of all tumor voxels results in a further improvement to treatment plan metrics. Median target coverage and median PCI take values of 0.88 and 0.76, respectively, while the median gradient index remains nearly unchanged. Hot and cold spots are substantially reduced, with median maximum and minimum tumor doses of 3.85 Gy and 27.1 Gy, respectively. Increasing the masking radius to 4 mm



provides an even larger improvement, with median target coverage and median PCI values of 0.98 and 0.82, respectively, and median maximum and minimum tumor doses of 22.65 and 7.8 Gy, respectively. This brings most treatment plan metrics close to their values when not applying any dose limits, with the exception of the median gradient index, which remains at an elevated value of 2.88.

### 4.3 | Optimization and treatment times

Both treatment plan optimization times and treatment times are affected by the inclusion of fOARs. Without fOARs the median time for generating a treatment plan is 0.45 min, or just under 30 s. The inclusion of fOARs increases the median optimization time for treatment plans to 5 min. Notably, optimization times are mostly dependent on the number and size of ROIs involved in the treatment planning, and are thus mostly unaffected by the various masking settings tested.

The median treatment time for patients when not using fOARs is 28 min, but with the inclusion of fOARs these times increase fourfold to 113 min. Much of this increase can be attributed to the presence of fMRI activation within and near the tumor mask, which give rise to complex treatment plans. While the masking of activations inside the tumors does not yield shorter treatment plans, the inclusion of 2 and 4 mm masking margins reduces median treatment times to 97 and 69 min, respectively.

### 4.4 | Effects of spatial smoothing

Figure 4 presents a comparison of treatment plan metrics for plans where fOARs were produced using spatial filters of 4 and 6 mm FWHM. It should be noted that 6 mm filters gave rise to substantially more active voxels than 4 mm filters, with a median ratio of 3 (range 1.6 – 12.3). This is to be expected, as the use of larger filters increases the detection power of the analysis, but also introduces uncertainty over the exact location of activations. Nevertheless, most treatment plan metrics yield comparable results for both of the filter sizes tested, particularly when not setting dose limits on fOARs.

When using fOARs, treatment quality metrics are consistently slightly worse for 6 mm filters than for 4 mm filters. Median target coverage and PCI are somewhat reduced for the 6 mm case, while median gradient indices are substantially higher than for 4 mm filters. These differences become more pronounced for larger margin sizes.

Comparison of tumor dose metrics is less straightforward. While the median minimum dose is slightly lower for 6 mm filters, the median maximum and mean doses are larger only for the cases when masking or margin

are not used, while becoming lower than the ones for 4 mm filters when a masking radius is used.

For both filter sizes, median treatment plan optimization times when using fOARs are unaffected by masking and margin settings, and are shorter for 4 mm filters than for 6 mm filters, with medians of 4 and 6 min, respectively. Notably, median treatment times from the plans generated using both filter sizes are not substantially different.

### 4.5 | Differences between subjects

Figure 5 presents individual treatment plan metrics obtained for each subject, illustrating that while there exists considerable variation in treatment plan quality at a subject level, the overall trends are shared by all subjects.

There is substantial subject-level variation in treatment quality metrics and in the relative benefits of applying masking and a margin on fOARs. For subjects 17904 and 19849, the inclusion of fOARs does not result in a substantial worsening of treatment plan quality, and masking bring quality metrics close to their values when no fOARs are applied. Conversely, for subjects 18975 and 19015 the use of fOARs results in a considerable reduction in treatment plan quality, and while masking provides a moderate improvement, quality metrics do not approach their values when fOARs are not used. Finally, subject 18582 is of particular interest, as they experience the greatest quality loss from the inclusion of fOARs, with target coverage and PCI being reduced by 0.37 and 0.38, respectively, yet disproportionately benefit from the use of masking, with the same metrics increasing by 0.35 and 0.33, respectively, when a 4 mm margin is used.

Tumor doses for different masking settings vary substantially across subjects. While subjects are differently affected by hot and cold spots, the use of masking and a margin around the tumor consistently reduces their presence for all subjects. Median maximum doses to fOARs for individual subjects can be as high as 13.6 Gy when dose constraints are not set, while the overall maximum dose observed on fOARs was 18.5 Gy. Nevertheless, setting dose constraints successfully limits the dose delivered to fOARs to 4 Gy or lower for all subjects.

Treatment plan optimization times show a strong dependence on tumor size, with larger tumors generally resulting in longer optimization times. Similarly, treatment times are generally higher for subjects with larger tumors.

## 5 | DISCUSSION

Our results show that including fMRI-derived fOARs in the treatment planning process successfully limits the

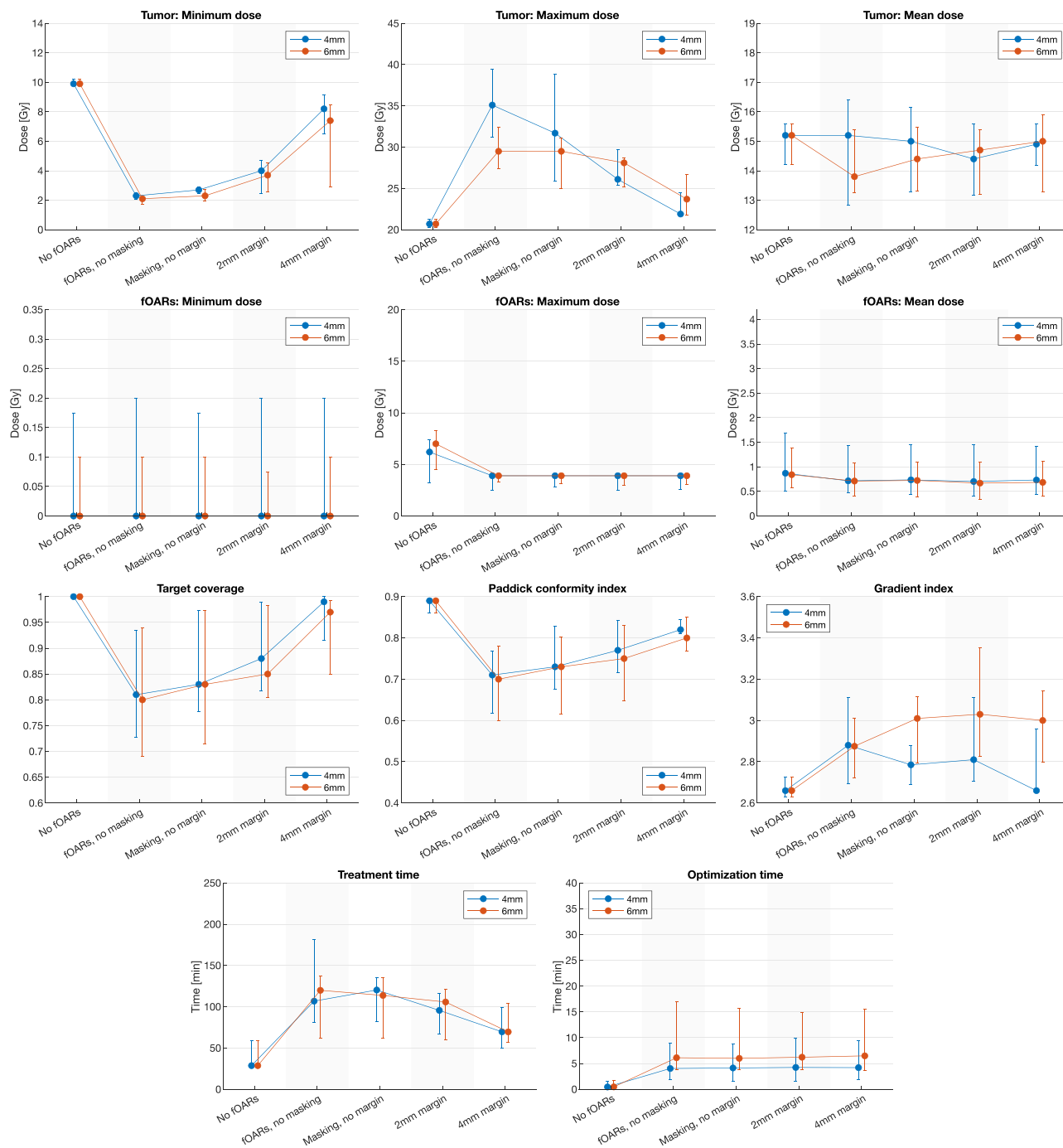


**FIGURE 4** Comparison of effects of different spatial smoothing filter sizes on metrics for treatment plans generated using different fOAR dose constraints and masking settings. First plot row: tumor dose metrics. Second plot row: fOAR dose metrics. Third and fourth plot rows: treatment plan metrics. The first column inside each plot (“No fOARs”) shows results when no dose limits are set for the fOARs, while the remaining four columns represent the various masking settings employed. Dots and error bars represent the median and interquartile range respectively. Plot data ranges are over subjects. fOARs, functional organs at risk.

radiation dose incident on the eloquent brain regions, while still resulting in clinically acceptable treatment plans. In general, masking out the fOARs in a margin around the tumor results in treatment treatment plan metrics close to the ones obtained without including fOARs. In terms of radiation, our results are in line

with previous work on using fOARs in treatment planning, showing that the eloquent brain areas receive substantially less radiation.<sup>14–16,19–23</sup>

Using the proposed method, it would be possible to incorporate fMRI-derived fOARs into the treatment planning protocol without requiring a large additional time

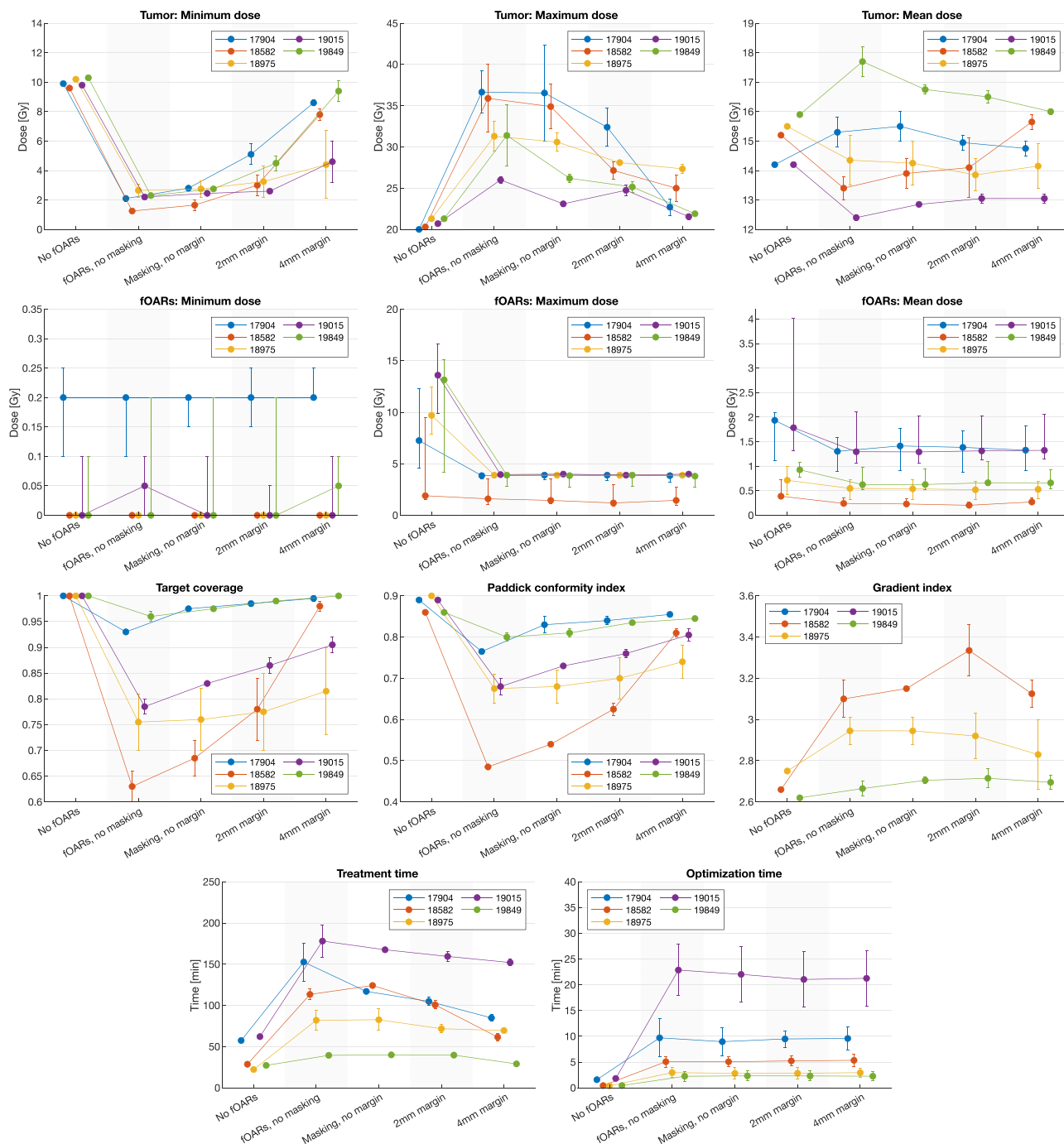


**FIGURE 5** Comparison of individual subject metrics for treatment plans generated using different fOAR dose constraints and masking settings. First plot row: tumor dose metrics. Second plot row: fOAR dose metrics. Third and fourth plot rows: treatment plan metrics. The first column inside each plot ("No fOARs") shows results when no dose limits are set for the fOARs, while the remaining four columns represent the various masking settings employed. Dots and error bars represent the median and interquartile range respectively. Plot data ranges are over smoothing filter sizes. fOARs, functional organs at risk.

investment. Collecting the fMRI data would require an additional 5–20 min in the MR scanner, depending on the number of tasks. While the preprocessing for a single subject can take approximately 100 min, most of this time is spent on preprocessing with fMRIPrep, and could be considerably reduced by using a different software tool or implementing a custom preprocessing pipeline.

From a user perspective, adding the fOARs in GammaPlan takes 1–3 min, while the optimization increases by 3–30 min, depending on the number and size of the targets and fOARs. From a treatment perspective, the treatment time increases from 20–60 min to 40–200 min, but this time can be substantially reduced to 20–160 min by the inclusion of a masking margin around

the targets. In addition, the use of cluster extent thresholding of the fMRI activation maps, as well as stricter voxel-level thresholding, can substantially reduce the number of brain activity clusters (fOARs), which would further reduce the optimization and treatment times. It should also be noted that the Lightning planner can be tuned to reduce the treatment time, at the cost of increasing the dose outside the target.

## 5.1 | Effects on patient quality of life

It is difficult to assess how using fOARs would affect the quality of life for the patients, as it would require a clinical study with and without fOARs in the treatment planning. Nevertheless, radiation induced damage to the healthy brain and its eloquent structures is a well-known and feared risk.<sup>12</sup> Sequelae such as motor dysfunction, cognitive impairment, loss of hearing or vision, cranial nerve dysfunction or hypopituitarism all have a negative impact on patients. These unwanted side-effects are therefore sought to be avoided as far as reasonably possible while still maintaining sufficient treatment levels of radiation to the target tissue.<sup>47</sup> In this work we show that treatment dose of target tissue can be maintained with a reduced dose of radiation to vulnerable areas in the vicinity of the tumor, which should be beneficial to the patients treated. A retrospective study evaluating SRS treatment outcomes over 8 years has shown that integrating tractography of the corticospinal tract into treatment planning contributed to reduction of motor complications, without compromising the obliteration rate for arteriovenous malformations adjacent to the corticospinal tract.<sup>48</sup> This required comparing treatments with and without additional risk organs.

## 5.2 | Limitations

Preprocessing and statistical analysis of fMRI data presents a large number of degrees of freedom.<sup>49,50</sup> A non-exhaustive list of these includes the specific preprocessing steps performed (e.g., head motion correction, co-registration, denoising, slice timing correction, distortion correction), the specific methods use for each of these, the statistical methods used (e.g., voxel-level inference vs. cluster extent inference, Bayesian models, etc.). It would be very interesting to investigate how different preprocessing settings, and different statistical analyses, affect the generated treatment plans, but GammaPlan requires that each treatment plan be generated and exported manually. It is therefore not possible for us to make use any scripting tools to perform a large number of analyses by looping through different subjects and a large number of different settings. For this reason, we have limited the number of presented analyses in this paper. Without this limitation we could present

results from many different settings for preprocessing and statistical analysis.

There is a degree of uncertainty inherent in the activation maps produced by fMRI. Activations frequently appear in regions other than expected from the task being performed, and may be disregarded. Furthermore, there is individual variability in the number, size, and location of activations,<sup>51</sup> which can be exacerbated by patient pathologies.<sup>39</sup> For these reasons, activation maps should be examined and thresholded by experienced neuroradiologists. This will however increase the planning time.

Stancanella et al.<sup>20</sup> refer to two sources of error in their procedure for generating fOARs from fMRI. The first is the threshold set by expert neuroradiologists to determine the location and extent of cortical activations. The second is the cumulative spatial imprecision resulting from chaining multiple registration steps. To these we must add that the data we used lacked any means for correcting susceptibility-based distortion. Although distortion correction without fieldmaps<sup>35</sup> has been shown to produce better result than no distortion correction, it is an experimental methodology, and fieldmap-based correction would have been preferred. In our case the registration between the fMRI data and the T1w volume will therefore not be perfect.

Our work was carried out on a dataset where structural MRI was acquired without gadolinium contrast, making it more difficult to clearly delineate tumor boundaries. However, as this work is a proof-of-concept where no actual patients were treated, the precise delineation of tumor borders is not essential.

## 5.3 | Experiences with GammaPlan

In our initial experiments with GammaPlan, each full activation map was treated as a single ROI, despite being composed of multiple unconnected components (clusters), as the RTSTRUCT format imposes no constraints on ROIs having to be single connected components. However, since GammaPlan implicitly creates a single connected volume as a triangulated mesh based on all contours belonging to the same ROI, such combined ROIs gave way to surface artifacts in the form of spurious connections and self-intersections. Instead, it is necessary to treat each individual connected component of the activation maps as a separate ROI, which was done in all reported experiments. However, this dramatically increases the number of ROIs that need to be managed in GammaPlan (up to anywhere from several dozen to almost two hundred in our case). This can be inconvenient, as for each ROI it is necessary to specify its type, that is, target or region of avoidance, with its corresponding target or maximum dose, respectively. While the ROI type can be specified in the DICOM metadata before loading them into GammaPlan, the dose settings



have to be set manually by the GammaPlan operator for each ROI.

Although treating each activation cluster as a single ROI removed most artifacts in GammaPlan, there were some remaining problems in approximately half of the 50 generated treatment plans. The imported 2D contours for fOARs look correct in the axial plane, but self intersections are visible in the coronal and sagittal planes. The 3D surface generated from these contours, used by the optimizer for dose calculations, occasionally intersects the tumor mask, resulting in incomplete target coverage and suboptimal treatment plans. This problem was present even in cases where fOARs were masked out within a radius around the tumor targets, which should preclude any overlap between fOARs and the tumor mask. As an independent validation of our workflow, we imported the same DICOM and RTSTRUCT files into the 3D Slicer software<sup>3</sup>, and observed that these problems were not present. The fact that the surface reconstruction in GammaPlan causes intersections between some fOARs and the tumor masks results in impaired treatment plans, and we believe that some of the reported treatment metrics would be further improved without this problem.

#### 5.4 | Clinical usage of fMRI in SRS

At Linköping University hospital, fMRI is part of the clinical protocol for brain tumor resection surgery in relevant cases, but not for SRS. There are at least two reasons why fMRI is not commonly used to generate fOARs for SRS. Firstly, automatic inverse planners have only recently become available for Gamma Knife SRS planning. To manually create 50 treatment plans while considering 80–180 fOARs for each would be prohibitively time-consuming. Secondly, creating a pipeline that analyzes the fMRI data and generates RTSTRUCT files was a non-trivial task. For instance, the conversion of data from NIfTI to DICOM format is substantially more involved than the opposite conversion. RTSTRUCT and DICOM are rather complex file formats, whereas neuroimaging researchers are mostly used to the simpler NIfTI file format. Our hope is that this work will increase the use of fOARs in SRS, and that our shared code can help other researchers and clinicians who want to continue our work.

One factor that could simplify the incorporation of fMRI data into clinical tumor treatment protocols is the adoption of DICOM Segmentation objects as a potential data format for the definition of dose optimization constraints. DICOM Segmentation objects provide a means for associating binary or fractional classification volumes to reference DICOM images, which

makes them ideally suited for storing brain activation maps in their native form, obviating the need for the cumbersome conversion step of activation maps into collections of contours required when using DICOM RT Structure Sets. Furthermore, the capacity to represent both binary and fractional classification volumes would allow them to store both thresholded and unthresholded activity maps, respectively. While DICOM RT Structure Sets are well suited for representing manual organ delineations, DICOM Segmentation objects are a better fit for representing the output of MRI processing pipelines and machine-generated organ delineations.

## 6 | CONCLUSION

Reducing the amount of gamma radiation incident on the eloquent regions of the brain can help minimize the risk of neurological complications after SRS, and improve the quality of life of patients. Task-based fMRI provides a way for localizing these regions. We have demonstrated that fMRI-derived fOARs can be incorporated into Gamma Knife SRS treatment planning to minimize the radiation dose incident on the eloquent regions of the brain, while maintaining acceptable treatment quality metrics. Although we have focused on task-based fMRI, similar pipelines can be set up to generate OARs from other MRI modalities, such as resting state fMRI and diffusion MRI, with the goal of reducing the radiation incident on specific brain networks and fiber tracts, respectively.

## ACKNOWLEDGMENTS

This study was performed in collaboration with Elekta Instrument AB (Stockholm, Sweden), and the authors are grateful for the opportunity of using the latest research version of Elekta Leksell GammaPlan which includes the inverse planner Lightning. We thank Håkan Nordström, Jonas Johansson, Björn Somell, Stella Riad and Kenneth Lau for sharing their valuable knowledge about GammaPlan. We thank Cyril Pernet et al. for collecting and sharing the used dataset.

This study was supported by CENIT at Linköping University, by the ITEA3 / VINNOVA funded project “Intelligence based iMprovement of Personalized treatment And Clinical workflow support” (IMPACT, grant 2018-02230), by LiU cancer at Linköping University, and by the ITEA3 / VINNOVA funded project “Automation, Surgery Support and Intuitive 3D visualization to optimize workflow in IGT SysTems”(ASSIST, grant 2021-01954). The authors did not receive any funding from Elekta Instrument AB.

## CONFLICT OF INTEREST STATEMENT

The authors declare no conflicts of interest.

<sup>3</sup> <https://www.slicer.org>

## REFERENCES

1. Leece R, Xu J, Ostrom QT, et al. Global incidence of malignant brain and other central nervous system tumors by histology, 2003–2007. *Neuro-oncol.* 2017;19:1553-1564.
2. Lunsford LD, Sheehan JP. *Intracranial Stereotactic Radiosurgery.* Thieme; 2009.
3. Fetcko K, Lukas RV, Watson GA, Zhang L, Dey M. Survival and complications of stereotactic radiosurgery: A systematic review of stereotactic radiosurgery for newly diagnosed and recurrent high-grade gliomas. *Medicine.* 2017;96:e8293.
4. Bokstein F, Blumenthal DT, Corn BW, et al. Stereotactic radiosurgery (SRS) in high-grade glioma: judicious selection of small target volumes improves results. *J Neurooncol.* 2016;126:551-557.
5. Skeie BS, Enger PØ, Brøgger J, et al. Gamma knife surgery versus reoperation for recurrent glioblastoma multiforme. *World Neurosurg.* 2012;78:658-669.
6. Weintraub D, Yen CP, Xu Z, Savage J, Williams B, Sheehan J. Gamma knife surgery of pediatric gliomas. *J Neurosurg Pediatr.* 2012;10:471-477.
7. Ruge MI, Tutunji J, Rueß D, et al. Stereotactic radiosurgery for treating meningiomas eligible for complete resection. *Radiat Oncol.* 2021;16:1-8.
8. Pinzi V, Biagioli E, Roberto A, et al. Radiosurgery for intracranial meningiomas: a systematic review and meta-analysis. *Crit Rev Oncol Hematol.* 2017;113:122-134.
9. Han MS, Jang WY, Moon KS, et al. Is fractionated gamma knife radiosurgery a safe and effective treatment approach for large-volume ( $> 10\text{ cm}^3$ ) intracranial meningiomas? *World Neurosurg.* 2017;99:477-483.
10. Kondziolka D, Lunsford LD, McLaughlin MR, Flickinger JC. Long-term outcomes after radiosurgery for acoustic neuromas. *N Engl J Med.* 1998;339:1426-1433.
11. China M, Vastani A, Hill CS, Tancu C, Grover PJ. Gamma Knife radiosurgery for cerebral arteriovenous malformations: a systematic review and meta-analysis. *Neurosurg Rev.* 2022;1-18.
12. Williams BJ, Suki D, Fox BD, et al. Stereotactic radiosurgery for metastatic brain tumors: a comprehensive review of complications. *J Neurosurg.* 2009;111:439-448.
13. Logothetis NK. What we can do and what we cannot do with fMRI. *Nature.* 2008;453:869-878.
14. Narayana A, Chang J, Thakur S, et al. Use of MR spectroscopy and functional imaging in the treatment planning of gliomas. *Br J Radiol.* 2007;80:347-354.
15. Kovács Á, Tóth L, Glavák C, et al. Integrating functional MRI information into conventional 3D radiotherapy planning of CNS tumors. Is it worth it? *J Neurooncol.* 2011;105:629-637.
16. Wang M, Ma H, Wang X, et al. Integration of BOLD-fMRI and DTI into radiation treatment planning for high-grade gliomas located near the primary motor cortex and corticospinal tracts. *Radiat Oncol.* 2015;10:1-7.
17. Hamilton R, Sweeney P, Pelizzari C, et al. Functional imaging in treatment planning of brain lesions. *Int J Radiat Oncol Biol Phys.* 1997;37:181-188.
18. Schulder M, Vega J, Narra V, et al. Functional magnetic resonance imaging and radiosurgical dose planning. *Stereotact Funct Neurosurg.* 2000;73:38-44.
19. Liu WC, Schulder M, Narra V, et al. Functional magnetic resonance imaging aided radiation treatment planning. *Med Phys.* 2000;27:1563-1572.
20. Stancaello J, Cavedon C, Francescon P, et al. BOLD fMRI integration into radiosurgery treatment planning of cerebral vascular malformations. *Med Phys.* 2007;34:1176-1184.
21. Pantelis E, Papadakis N, Verigos K, et al. Integration of functional MRI and white matter tractography in stereotactic radiosurgery clinical practice. *Int J Radiat Oncol Biol Phys.* 2010;78:257-267.
22. Conti A, Pontoriero A, Ricciardi GK, et al. Integration of functional neuroimaging in CyberKnife radiosurgery: feasibility and dosimetric results. *Neurosurg Focus.* 2013;34:E5.
23. De Martin E, Duran D, Ghielmetti F, et al. Integration of functional magnetic resonance imaging and magnetoencephalography functional maps into a CyberKnife planning system: feasibility study for motor activity localization and dose planning. *World Neurosurg.* 2017;108:756-762.
24. Maruyama K, Kamada K, Shin M, et al. Integration of three-dimensional corticospinal tractography into treatment planning for gamma knife surgery. *J Neurosurg.* 2005;102:673-677.
25. Maruyama K, Kamada K, Shin M, et al. Optic radiation tractography integrated into simulated treatment planning for Gamma Knife surgery. *J Neurosurg.* 2007;107:721-726.
26. Maruyama K, Koga T, Kamada K, et al. Arcuate fasciculus tractography integrated into Gamma Knife surgery. *J Neurosurg.* 2009;111:520-526.
27. Koga T, Maruyama K, Kamada K, et al. Outcomes of diffusion tensor tractography-integrated stereotactic radiosurgery. *Int J Radiat Oncol Biol Phys.* 2012;82:799-802.
28. Gavin CG, Sabin HI. Stereotactic diffusion tensor imaging tractography for Gamma Knife radiosurgery. *J Neurosurg.* 2016;125:139-146.
29. J., Sjöland, Riad S, Hennix M, Nordström H. A linear programming approach to inverse planning in Gamma Knife radiosurgery. *Med Phys.* 2019;46:1533-1544.
30. Paddick I, Grishchuk D, Dimitriadis A. IntuitivePlan inverse planning performance evaluation for Gamma Knife radiosurgery of AVMs. *J Appl Clin Med Phys.* 2020;21:90-95.
31. Zeverino M, Marguet M, Zulliger C, et al. Novel inverse planning optimization algorithm for robotic radiosurgery: first clinical implementation and dosimetric evaluation. *Physica Med.* 2019;64:230-237.
32. Pernet CR, Gorgolewski KJ, Job D, Rodriguez D, Whittle I, Wardlaw J. A structural and functional magnetic resonance imaging dataset of brain tumour patients. *Sci Data.* 2016;3:1-6.
33. Gorgolewski KJ, Storkey AJ, Bastin ME, Whittle I, Pernet C. Single subject fMRI test-retest reliability metrics and confounding factors. *Neuroimage.* 2013;69:231-243.
34. Menze BH, Jakab A, Bauer S, et al. The multimodal brain tumor image segmentation benchmark (BRATS). *IEEE Trans Med Imaging.* 2014;34:1993-2024.
35. Esteban O, Markiewicz CJ, Blair RW, et al. fMRIPrep: a robust preprocessing pipeline for functional MRI. *Nat Methods.* 2019;16:111-116.
36. Gorgolewski KJ, Auer T, Calhoun VD, et al. The brain imaging data structure, a format for organizing and describing outputs of neuroimaging experiments. *Sci Data.* 2016;3:1-9.
37. Fischl B. FreeSurfer. *Neuroimage.* 2012;62:774-781.
38. Jenkinson M, Beckmann CF, Behrens TE, Woolrich MW, Smith SM. FSL. *Neuroimage.* 2012;62:782-790.
39. Silva MA, See AP, Essayed WI, Golby AJ, Tie Y. Challenges and techniques for presurgical brain mapping with functional MRI. *Neuroimage Clin.* 2018;17:794-803.
40. Stippich C, Blatow M, Alzamora MG. Task-based presurgical functional MRI in patients with brain tumors. *Clinical functional MRI.* Springer; 2022:121-195.
41. Bogomolny DL, Petrovich NM, Hou BL, Peck KK, Kim MJ, Holodny AI. Functional MRI in the brain tumor patient. *Top Magn Reson Imaging.* 2004;15:325-335.
42. Law MY, Liu B. DICOM-RT and its utilization in radiation therapy. *Radiographics.* 2009;29:655-667.
43. Van der Walt S, Schönberger JL, Nunez-Iglesias J, et al. scikit-image: image processing in Python. *PeerJ.* 2014;2:e453.
44. Mason D. SU-E-T-33: pydicom: an open source DICOM library. *Med Phys.* 2011;38:3493-3493.
45. Paddick I. A simple scoring ratio to index the conformity of radiosurgical treatment plans. *J Neurosurg.* 2000;93:219-222.

46. Paddick I, Lippitz B. A simple dose gradient measurement tool to complement the conformity index. *J Neurosurg.* 2006;105:194-201.
47. Lambrecht M, Eekers DBP, Alapetite C, et al. Radiation dose constraints for organs at risk in neuro-oncology; the European Particle Therapy Network consensus. *Radiother Oncol.* 2018;128:26-36.
48. Koga T, Shin M, Maruyama K, et al. Integration of corticospinal tractography reduces motor complications after radiosurgery. *Int J Radiat Oncol Biol Phys.* 2012;83:129-133.
49. Carp J. The secret lives of experiments: methods reporting in the fMRI literature. *Neuroimage.* 2012;63:289-300.
50. Carp J. On the plurality of (methodological) worlds: estimating the analytic flexibility of FMRI experiments. *Front Neurosci.* 2012;6:149.
51. Bennett CM, Miller MB. How reliable are the results from functional magnetic resonance imaging? *Ann N Y Acad Sci.* 2010;1191:133-155.

## SUPPORTING INFORMATION

Additional supporting information can be found online in the Supporting Information section at the end of this article.

**How to cite this article:** Abramian D, Blystad I, Eklund A. Evaluation of inverse treatment planning for gamma knife radiosurgery using fMRI brain activation maps as organs at risk. *Med Phys.* 2023;50:5297–5311.  
<https://doi.org/10.1002/mp.16660>

## APPENDIX: fMRI PREP PREPROCESSING

The exact function call used for fMRIPrep was  
`fmriprep --random-seed 100 --skull-strip-t1w  
 auto --output-spaces T1w --use-syn-sdc  
 --fs-no-reconall --fs-license-file  
 /license.txt /data /out participant.`  
 The detailed, auto-generated description of the processing steps carried out by fMRIPrep is provided in the [Supplementary Material](#).